

1 **Bacterial Footprints in Elastic Pillared Microstructures**

2 Arturo Susarrey-Arce,<sup>\*,†,○</sup> José Federico Hernández-Sánchez,<sup>\*,‡,○</sup> Marco Marcello,<sup>¶</sup>  
 3 Yuri Diaz-Fernandez,<sup>†</sup> Alina Oknianska,<sup>§</sup> Ioritz Sorzabal-Bellido,<sup>†</sup> Roald Tiggelaar,<sup>||</sup> Detlef Lohse,<sup>⊥,○</sup>  
 4 Han Gardeniers,<sup>#,○</sup> Jacco Snoeijer,<sup>\*,⊥</sup> Alvaro Marin,<sup>⊥</sup> and Rasmita Raval<sup>\*,†</sup>

5 <sup>†</sup>Open Innovation Hub for Antimicrobial Surfaces at the Surface Science Research Centre and Department of Chemistry, University  
 6 of Liverpool, Oxford Street, Liverpool L69 3BX, United Kingdom

7 <sup>‡</sup>Division of Physical Sciences and Engineering and Clean Combustion Research Center, King Abdullah University of Science and  
 8 Technology, Thuwal 23955-6900, Saudi Arabia

9 <sup>¶</sup>Institute of Integrative Biology, University of Liverpool, Biosciences Building, Liverpool L69 7ZB, United Kingdom

10 <sup>§</sup>School of Health Sciences, Liverpool Hope University, Hope Park, Liverpool L16 9JD, United Kingdom

11 <sup>||</sup>NanoLab Cleanroom, MESA+ Institute for Nanotechnology, University of Twente, P.O. Box 217, Enschede 7500AE, The  
 12 Netherlands

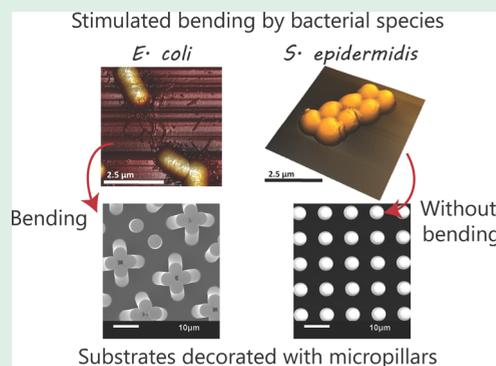
13 <sup>⊥</sup>Physics of Fluids Group, MESA+ Institute for Nanotechnology, J.M. Burgers Centre for Fluid Dynamics, University of Twente,  
 14 P.O. Box 217, Enschede 7500AE, The Netherlands

15 <sup>#</sup>Mesoscale Chemical Systems, MESA+ Institute for Nanotechnology, University of Twente, P.O. Box 217, Enschede 7500AE, The  
 16 Netherlands

17 **S Supporting Information**

18 **ABSTRACT:** Soft substrates decorated with micropillar arrays are known to  
 19 be sensitive to deflection due to capillary action. In this work, we demonstrate  
 20 that micropillared epoxy surfaces are sensitive to single drops of bacterial  
 21 suspensions. The micropillars can show significant deformations upon  
 22 evaporation, just as capillary action does in soft substrates. The phenomenon  
 23 has been studied with five bacterial strains: *S. epidermidis*, *L. sakei*, *P.*  
 24 *aeruginosa*, *E. coli*, and *B. subtilis*. The results reveal that only droplets  
 25 containing motile microbes with flagella stimulate micropillar bending, which  
 26 leads to significant distortions and pillar aggregations forming dimers, trimers,  
 27 and higher order clusters. Such deformation is manifested in characteristic  
 28 patterns that are left on the microarrayed surface following evaporation and  
 29 can be easily identified even by the naked eye. Our findings could lay the  
 30 ground for the design and fabrication of mechanically responsive substrates,  
 31 sensitive to specific types of microorganisms.

32 **KEYWORDS:** bacteria, bending, elastic micropillars, capillarity, responsive substrates

33 **INTRODUCTION**

34 The fabrication of materials that are sensitive to physical,  
 35 chemical, or biological stimuli has opened opportunities for the  
 36 development of a wide variety of technological applications  
 37 such as switchable adhesion, mechanosensing, and stimuli-  
 38 responsive materials.<sup>1–6</sup> In particular, the design of biomimetic  
 39 structures,<sup>3,7</sup> inspired by natural systems, has been a powerful  
 40 tool in the implementation of smart, artificial systems.<sup>8,9</sup> In this  
 41 respect, the use of topographic surfaces is particularly  
 42 interesting, with natural systems utilizing physical structures,  
 43 from the nano- to the macroscale, to deliver functions such as  
 44 superhydrophobicity, adhesion, and antibiofouling as demon-  
 45 strated by the lotus leaf, shark skin, and gecko feet.<sup>4,7,9–13</sup>

46 There has been particular interest in developing mechan-  
 47 ically responsive systems.<sup>8,14</sup> An excellent example is the  
 48 mechanical response of micropillar arrays upon drying of water

(or water-based solutions).<sup>15–26</sup> When water droplets  
 49 evaporate on relatively soft elastic microstructured surfaces,  
 50 capillary action can generate a significant force that is able to  
 51 bend the soft micropillars. Depending on the geometry of the  
 52 arrays, the capillary and elastic forces can form different pillar  
 53 assemblies.<sup>15,16</sup> The complexity of the assemblies varies with  
 54 the pillar height and the interpillar distance. For example, large  
 55 periodic chiral aggregates can be formed when the micropillars  
 56 are higher and closer to each other. Each cluster of aggregates  
 57 has a different potential to store elastic energy, embody  
 58 information, enhance adhesion, or capture particles.<sup>17,18</sup> 59

**Received:** May 31, 2018

**Accepted:** October 15, 2018

**Published:** October 15, 2018

60 The demonstration of mechanically responsive topographic  
 61 surfaces to bacterial stimuli during evaporation of small  
 62 droplets is of great interest and has not been demonstrated  
 63 before. Furthermore, the deflections seen in our systems are  
 64 significant, leading to pillar aggregations into dimers, trimers,  
 65 and higher order clusters. Recently, the formation of biofilm  
 66 strings and networks between topographic pillars has been  
 67 demonstrated in liquid media;<sup>27</sup> however, the mechanical  
 68 response of the pillars to bacterial presence upon evaporation  
 69 is not observed. Chew and coauthors have shown small  
 70 deflections of micropillared surfaces in response to the  
 71 differential pressure exerted by biofilm growth within a growth  
 72 chamber over a 24 h period,<sup>28</sup> while Biais<sup>29</sup> and Ng<sup>30</sup> et al.  
 73 have investigated the interaction of bacterial pili with pillared  
 74 structures.

75 Here, we demonstrate how epoxy-made soft surfaces  
 76 containing micropillar arrays interact with suspensions of  
 77 different bacterial species. Our results suggest that the presence  
 78 of motile bacteria with flagella drastically increases the  
 79 mechanical response of the pillars, actively bending soft  
 80 topographical substrates in the area contained within the  
 81 contact line. In contrast, solutions containing nonmotile  
 82 bacteria do not generate such responses. We attribute this to  
 83 the ability of motile bacteria to interact with each other and  
 84 with their topographical environment. Importantly, the  
 85 response of the microarray is sensitive to the type and  
 86 concentration of bacteria in the solution. These promising  
 87 results could lay the foundation for the development of devices  
 88 that are selectively responsive to specific microorganisms,  
 89 paving the way to construct smart, fast, and cost-effective  
 90 diagnostic tools.

## 91 ■ RESULTS AND DISCUSSION

92 One of the key parameters in the mechanical response of soft  
 93 micropillar arrays is the aspect ratio of a single pillar. We  
 94 investigated the effect of the pillar aspect ratio by fabricating  
 95 regular patterns of cylindrical pillars with a constant diameter  
 96 ( $5\ \mu\text{m}$ ) and interspacing ( $5\ \mu\text{m}$ ) and with variable height  
 97 (from  $5$  to  $45\ \mu\text{m}$ ). The patterns were created on epoxy resin  
 98 using a method described before<sup>31–35</sup> based on casting  
 99 uncured epoxy on a negative polydimethylsiloxane (PDMS)  
 100 mold, followed by curing and mechanically removing of the  
 101 mold. The micropatterns were transferred efficiently, with a  
 102 high degree of fidelity, as shown by scanning electron  
 103 microscopy (SEM) imaging (Figure 1 and Figure S1).

104 These microstructured substrates can be susceptible to  
 105 elastocapillary forces in the presence of pure liquids. Therefore,  
 106 we evaluated the effect of pure water over a surface decorated  
 107 with micropillars with lengths varying from  $5$  to  $45\ \mu\text{m}$  (Figure  
 108 1) during the evaporation of water droplets (Figure 1). In  
 109 these experiments, the liquid filled up the space between the  
 110 pillars, resulting in an almost square-shaped droplet contour.  
 111 Once the droplet spreads on the substrate, the liquid contact  
 112 line is blocked by the pillared structure and remains  
 113 immobilized (pinned) for the rest of the drying process.<sup>31</sup>  
 114 Figure 1b shows that after complete evaporation, there is  
 115 almost no trace of the droplet, except at the droplet contour,  
 116 where lines of pillars were bent by capillary action at the  
 117 contact line shown in Video S1.<sup>18–23,31</sup>

118 In the systems studied, the pillar lattice was kept constant  
 119 (i.e.,  $l = d = 5\ \mu\text{m}$ ), but different pillar heights ( $h$ ) ranging from  
 120  $h = 5$  to  $45\ \mu\text{m}$  were fabricated. Thus, a range of  
 121 micropatterned surfaces were generated with different aspect

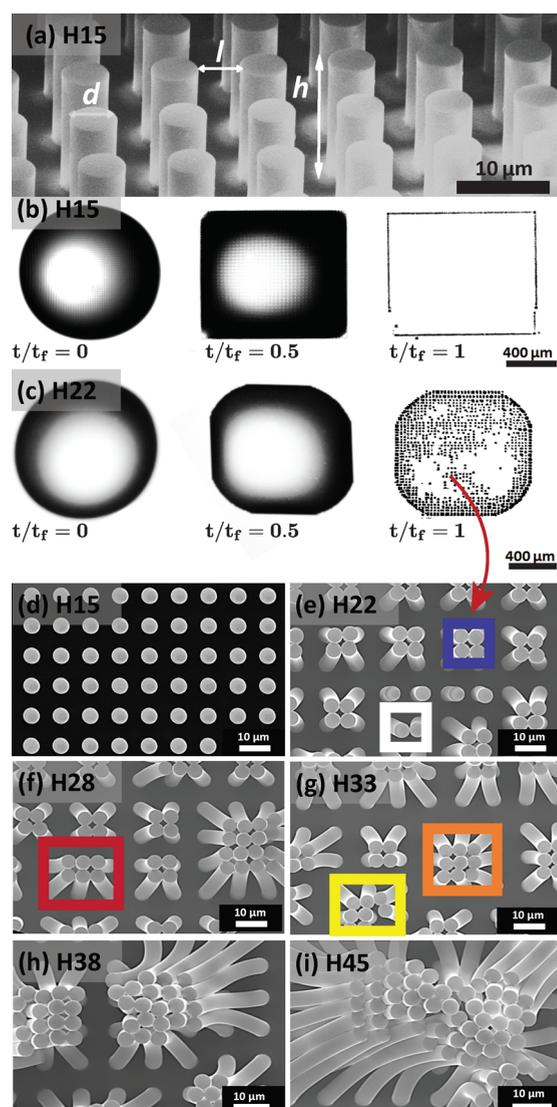


**Figure 1.** (a) Representative SEM image of pillared structure (H15), showing the topographic descriptors for the array. The pillars have a cylindrical shape and a height ( $h$ ) of  $15\ \mu\text{m}$  and a diameter ( $d$ ) of  $5\ \mu\text{m}$  forming a square lattice with an interpillar distance ( $l$ ) =  $5\ \mu\text{m}$ . (b) Pure water droplet evaporating on the H15 substrate with micropillars leaving a distinct square-shaped contact line with no perturbation of pillars within this contour. (c) Pure water droplet evaporating on the H22 substrate with micropillars leaving a distinct shaped contact line pattern with significant modification of the micropillars within the contact line boundary. Time needed is represented in a dimensionless form as the ratio between the elapsed time ( $t$ ) and the final evaporation time ( $t_f$ ). (d–i) Pillared structures with constant ( $d = 5\ \mu\text{m}$ ) and different pillar heights ( $h$ ) of (d)  $15\ \mu\text{m}$  (H15), (e)  $22\ \mu\text{m}$  (H22), (f)  $28\ \mu\text{m}$  (H28), (g)  $33\ \mu\text{m}$  (H33), (h)  $38\ \mu\text{m}$  (H38), and (i)  $45\ \mu\text{m}$  (H45). SEM images are presented for the different heights after evaporation of pure water droplets, probing the sensitivity of the structures to pure elastocapillary bending.

ratios (i.e.,  $h/d = 3$  to  $h/d = 9$ ). For large aspect ratio  
 122 structures, we observed significant perturbation of the  
 123 micropillars in the area within the contact line boundary.  
 124 Imaging at low magnifications, or even examination by the  
 125 naked eye, revealed that the inner part of the pattern was  
 126 opaque, suggesting that the whole array of pillars inside the  
 127 dried droplet perimeter was modified (Figure 1c). Higher  
 128 magnification SEM imaging showed that this optical contrast  
 129

130 effect was caused by local bending of the micropillars (Figure  
131 1d–i), with the pillars bent toward each other forming clusters  
132 and adopting complex geometries, e.g., dimer (white box),  
133 tetramer (blue box), hexamer (red box), octamer (yellow box),  
134 and nonamer (orange box). Similar effects have been reported  
135 before for larger pillar aspect ratios<sup>18,24,25</sup> and were attributed  
136 to the elastocapillary coalescence of the flexible structures.<sup>15,18</sup>

137 In our experiments, as the aspect ratio decreased, the clusters  
138 contained lower numbers of aggregated pillars until a critical  
139 aspect ratio  $h/d = 3$ , for which no clusters were observed in the  
140 inner part of the droplet (Figure 1d).

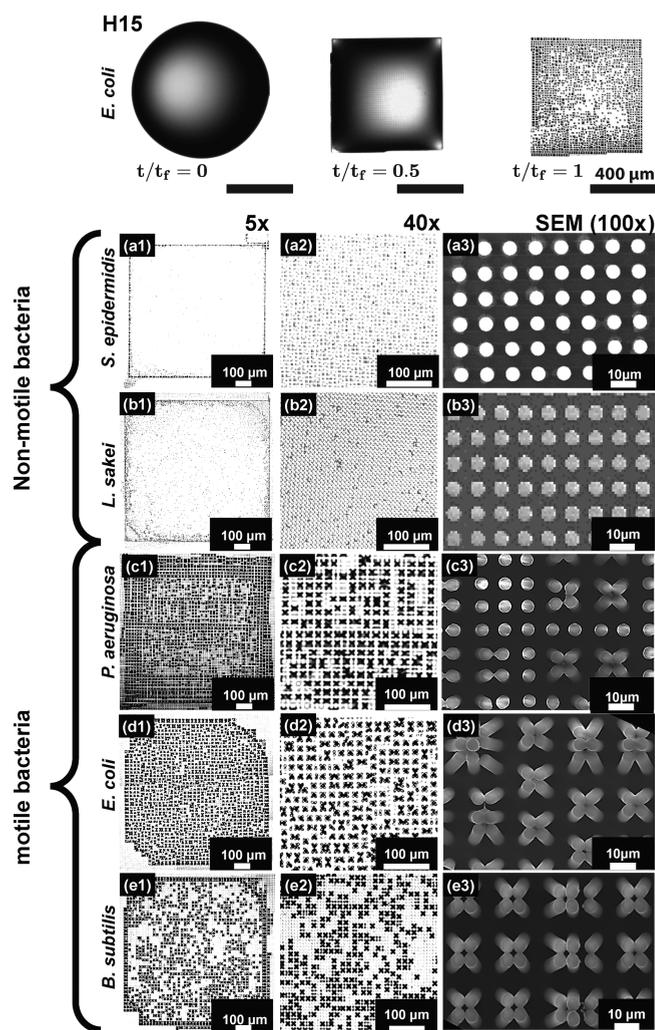
141 The deformation of the pillars, upon water evaporation, is  
142 induced by the surface tension ( $\gamma$ ) of the water/air meniscus  
143 connecting the pillars, and the corresponding force scales as  $F_c$   
144  $\sim \gamma r$ , where  $r = d/2$  is the pillar radius.<sup>21,36</sup> The natural  
145 elasticity of the pillars resists deformation with an elastic force  
146  $F_E \sim Elr^4/h^3$ , where  $E$  is the Young modulus and  $l$  the  
147 interpillar distance.<sup>18</sup> This expression is analogous to the usual  
148 beam theory for slender objects, showing that the resistance to  
149 bending decreases strongly when the pillar height increases. If  
150 we define the pillar bending sensitivity as the ratio of capillary  
151 and elastic forces,  $F_c/F_E = \gamma/El(h/r)^3$ , we can conclude that it  
152 is directly proportional to the cubic power of the pillar aspect  
153 ratio  $h/r$ ; i.e., slender pillars are more prone to be bent by  
154 surface tension, while wide pillars tend to be more stable.

155 Under our experimental conditions, no pillar coalescence is  
156 observed in the area within the contact line boundary from  
157 pure water when the aspect ratio is below  $h/d = 3$ ,<sup>31</sup> suggesting  
158 that this is the critical aspect ratio threshold for which capillary  
159 action equals restoration mechanical stress on the micropillars.  
160 It is important to note that in this analysis, we are not  
161 considering the effect of the contact line. This effect is  
162 expected to have an enhanced deforming effect, but an  
163 accurate evaluation of this factor is beyond existing  
164 phenomenological modeling capabilities and will be the subject  
165 of future studies. Consequently, all of the results described  
166 below applies exclusively to the inner part of the dried pattern  
167 left by the droplet, ignoring possible contact line effects.

168 **Bacterial-Triggered Coalescence of Pillars.** From the  
169 elastocapillary assay discussed in the previous section, we  
170 identified the critical region within the topographic parameter  
171 space where the micropillared structure is able to resist  
172 capillary deformation in the presence of pure water droplets.  
173 Such a surface opens up the possibility to sense the presence of  
174 a second entity introduced into water (i.e., bacterial cells),  
175 which could induce a response in its own right. This critical  
176 structure corresponds to an aspect ratio  $h/d \approx 3$  and pillar  
177 height  $h = 15 \mu\text{m}$  (H15, Figure 1d), as discussed in the  
178 previous section.

179 We, therefore, investigated the drying process of droplets  
180 containing different bacteria species over the H15 pillared  
181 structures. Similar to the case of pure water droplets, a pinned  
182 square drop shape is found. However, the patterns observed  
183 within the contact line formed after complete evaporation of  
184 the droplets were surprisingly different for some bacteria as  
185 clearly observed in Video S2.

186 Five different bacterial species, with a wide range of  
187 morphological and biological characteristics were investigated:  
188 *S. epidermidis*, *L. sakei*, *P. aeruginosa*, *E. coli*, and *B. subtilis*. The  
189 patterns formed after evaporation of droplets containing  
190 different bacteria on H15 pillar substrates (Figure 2) can be  
191 classified in two main groups: one group displaying significant  
192 bending of the pillars within the pattern (*P. aeruginosa*, *E. coli*,



193 **Figure 2.** Typical patterns left over H15 substrates after the  
194 evaporation of different bacterial species: (a1–a3) *S. epidermidis*,  
195 (b1–b3) *L. sakei*, (c1–c3) *P. aeruginosa*, (d1–d3), *E. coli*, (e1–e3) *B.*  
196 *subtilis*. Here, the concentration of the different bacterial species is  $10^7$   
197 CFU/mL. The different columns correspond to different degrees of  
198 magnifications: 5 $\times$  (left column), 40 $\times$  (central column) by using a  
199 confocal microscope, and >100 $\times$  with SEM (right column).

200 and *B. subtilis*) and another group that does not induce any  
201 responsive bending of the pillars in the center of the dried  
202 patterns (*S. epidermidis* and *L. sakei*). These distinct behaviors  
203 could be observed even by the naked eye in the form of a local  
204 change in contrast at the surface (Figure 2, 5 $\times$ ). At higher  
205 magnifications, the difference is clearly revealed to be  
206 associated with the coalescence of adjacent pillars (Figure 2,  
207 40 $\times$  and SEM (100 $\times$ )).

208 We attempted to correlate these results to the general  
209 characteristics of the bacterial species used in this work (Table  
210 1). Atomic force microscopy (AFM) imaging confirmed the  
211 expected size and cell morphology for these bacteria: Gram-  
212 negative (–) *P. aeruginosa* and *E. coli* as well as Gram-positive  
213 (+) *B. subtilis* and *L. sakei* present a rod-like shape, while  
214 Gram-positive (+) *S. epidermidis* has a spheroidal shape  
215 (Figure S2). In addition, *L. sakei* and *S. epidermidis* are not  
216 motile (no flagella present), while the other three strains have  
217 flagella. From these considerations, we can conclude that the  
218 different pattern types showed in Figure 2 (bending vs  
219 nonbending) cannot be explained considering bacteria cell

**Table 1. General Characteristics of the Different Bacterial Strains Used in the Study<sup>a</sup>**

strain	gram	shape	$L \times W_a$ ( $\mu\text{m}^2$ )	flagella
(a) <i>P. aeruginosa</i>	–	rod	$1.4(\pm 0.2) \times 0.8(\pm 0.2)$	yes
(b) <i>E. coli</i>	–	rod	$1.7(\pm 0.2) \times 0.9(\pm 0.2)$	yes
(c) <i>B. subtilis</i>	+	rod	$1.8(\pm 0.4) \times 0.80(\pm 0.2)$	yes
(d) <i>L. sakei</i>	+	rod	$1.5(\pm 0.4) \times 0.8(\pm 0.2)$	no
(e) <i>S. epidermidis</i>	+	spherical	$1.3(\pm 0.3) \times 1.3(\pm 0.3)$	no

<sup>a</sup>AFM images of cells are presented in Figure S2.

213 morphology only. Similarly, the stiffness of the cell envelop  
214 does not appear to play a critical role, with rigid Gram-positive  
215 bacteria and softer Gram-negative bacteria distributed among  
216 both pattern groups.

217 Interestingly, the different response of the microstructures  
218 upon evaporation of the bacterial solutions correlates with the  
219 presence or absence of flagella. Bacteria with flagella clearly  
220 induce a bending response in the H15 pillars, while  
221 nonflagellated bacteria are unable to bend the pillars when  
222 used at the same bacterial concentration.

223 For the bacteria that induce a mechanical response, a  
224 concentration dependence is observed, with deformation of  
225 pillar clusters at the center of the dried droplet observed for  
226 bacteria concentrations between  $10^7$  CFU/mL and  $10^9$  CFU/  
227 mL, while none is observed for lower bacteria concentrations  
228 ( $10^5$  CFU/mL). At low concentrations, only the perimeter  
229 near the corners of the dried square pattern presented  
230 coalescence of the pillars (Figure 3a–c). This can be attributed  
231 to the coffee-stain-like effect, able to drag bacterial cells toward  
232 the droplet contact line, increasing the local concentration of  
233 bacteria during evaporation.<sup>31</sup> Interestingly, bacterial cells  
234 without flagella confirm the absence of responsivity at different  
235 cell concentrations (Figure 3d–f).

No clear correlation was observed between bacterial species 236  
and the cluster symmetries obtained (e.g., dimer, trimer, 237  
tetramer, etc.). However, the data suggests that the assemblies 238  
emerge due to perturbation of the balance between capillary 239  
forces and elastic restoration forces in the presence of bacteria 240  
with flagella. In the next section, we discuss a possible 241  
mechanism for this distinctive behavior. 242

**Possible Origin of Bacteria-Induced Coalescence.** In 243  
the previous sections, we determined the critical pillar aspect 244  
ratio, below which surface tension forces were not able to 245  
induce pillar coalescence in pure water. Interestingly, the 246  
responsivity is dramatically enhanced when the droplets 247  
contain flagellated bacteria. While the bending process at the 248  
perimeter of the contact line appears similar in both cases, 249  
coalescence within the central area is triggered at smaller 250  
aspect ratios by the presence of bacteria with flagella. This 251  
enhanced pillar bending effect results in characteristic patterns 252  
on the substrate, distinct for motile and nonmotile bacteria. 253

The possible origin of the enhanced pillar bending may be 254  
related to the ability of the bacteria with flagella to adhere to 255  
more than one pillar (Figure S3), thus connecting adjacent 256  
pillars and inducing a mechanical deformation. In the presence 257  
of bacteria with flagella, we observed, at SEM, after drying, 258  
structures bridging bent pillars, while nonflagellated bacteria 259  
appeared attached to single pillars. The morphology of the 260  
single bacterial cells cannot be distinguished, probably due to 261  
distortions on the cell envelop after evaporation, in the absence 262  
of fixation. 263

These effects can also be understood by comparing the 264  
length scales of bacterial structures and pillar interspacing 265  
distances. The average size of the capsule for a single bacterial 266  
cell is below  $2 \mu\text{m}$  (Table 1), while flagella can reach tens of 267  
 $\mu\text{m}$  beyond the outer cell membrane.<sup>37</sup> Considering that in our 268  
microstructured surfaces the interpillar distance was  $5 \mu\text{m}$ , 269  
bacteria without flagella will predominantly fall between the 270

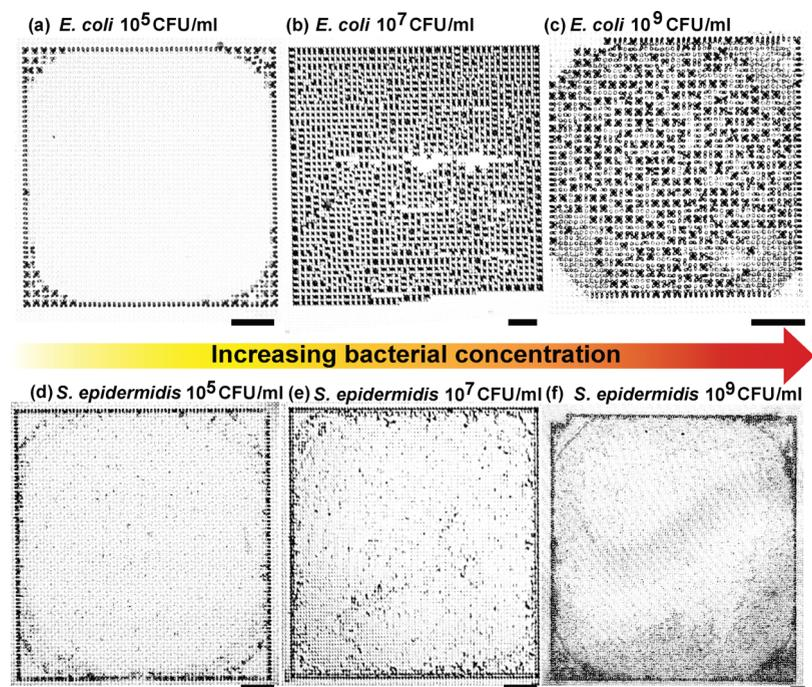
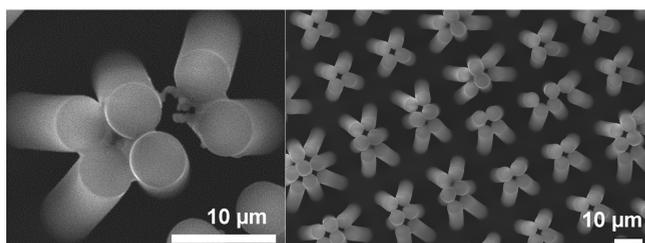


**Figure 3.** Effect of bacteria concentration on the bending pattern for *E. coli* and *S. epidermidis* on the H15 pillared substrate. Representative optical microscopy images for (a)  $10^5$  CFU/mL, (b)  $10^7$  CFU/mL, and (c)  $10^9$  CFU/mL. Scale bar in panels a–f is  $100 \mu\text{m}$ .

pillars or strongly adhere<sup>38</sup> to single pillars. On the other hand, bacteria with flagella,<sup>32</sup> in which appendage sizes exceed the interpillar distance, can potentially interact with more than one pillar, leading to the observed pillar deformation. In support of this, we found evidence of bacterial matter residing between the bent pillars, after complete evaporation of droplets containing flagellated bacteria (Figure 4). Non-flagellated bacteria, on the other hand, are found attached to individual pillars only, forming nonconnecting structures (see Figures S4–S7).

### *B. subtilis*



### *E. coli*

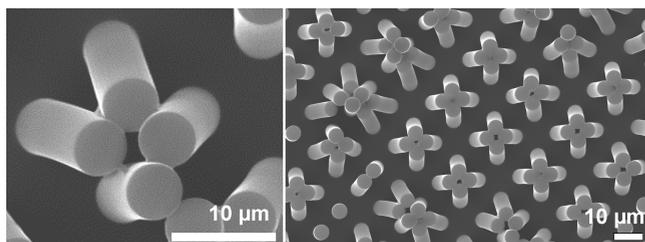


**Figure 4.** Representative SEM images of H15 pillared structures after drying of bacterial suspensions, showing motile bacteria (*B. subtilis* and *E. coli*) bridging the bent pillars. The concentration of the different bacterial species is  $10^7$  CFU/mL.

Although a more detailed investigation of bacterial behavior during the actual drying process is necessary to confirm the hypothesis proposed, our results support the potential use of pillared soft substrates to discriminate between motile and nonflagellated bacteria using a cost-effective and immediate assay based on droplet-drying, which can be performed and quickly analyzed by the naked eye. In addition, discrimination of bacterial concentration is also possible, with only samples containing concentrations above a critical threshold producing a response. We envision that by tuning the properties of the substrates, a more subtle differentiation between different microorganisms and different bacterial concentrations could be achieved in the future with this presented novel, easy to fabricate, and cost-effective technology.

## CONCLUSIONS

We show that soft micropillared surfaces can be tailor-made sensitive to the presence of isolated bacterial cells in a single drop. The evaporation of water droplets and bacterial suspensions over fabricated micropillar arrays leads to very distinct micropillar deformations and patterns. Once the threshold for elastocapillary pillar coalescence is found, we observe that only bacteria with flagella can promote pillar coalescence. Such responsive micropillared surfaces could provide a platform for the development of fast and cost-effective self-responsive surfaces for bacterial detection and differentiation.

## EXPERIMENTS AND METHODS

The epoxy micropillars were fabricated by casting EPO-TEK OG142-13 from Epoxy Technology into a negative replica PDMS mold, as described.<sup>31,32</sup> After the resin was casted, a 1.1 mm thick glass slide was placed over the mold and placed below an ultraviolet light for 20 min until the epoxy pillar was cured. The epoxy micropillars were mechanically removed from the mold. The SEM images of the epoxy pillars are shown in Figure S1. After the sample preparation, we measured the Young modulus ( $E$ ) of the bulk material and the micropillar via an axial compression test. The  $E$  value for the bulk material was  $1 \pm 0.3$  GPa, and the  $E$  value for the H15 substrate was  $0.5 \pm 0.2$  GPa.

Bacterial cultures were performed following recommended growing conditions for each species. *P. aeruginosa* ATCC-8626, *E. coli* ATCC-10798, and *S. epidermidis* ATCC-12228 were grown overnight at 37 °C in liquid broth medium (Oxoid Ltd., Thermo Fisher). *B. subtilis* subsp. *subtilis* ATCC-6051 and *L. sakei* DSMZ-20017 were grown overnight at 30 °C in MRS broth medium from Oxoid Ltd., Thermo Fisher. All of the cells cultures were then centrifuged and redispersed in sterile deionized water two times, finally adjusting the bacterial concentration to  $10^7$  colony-forming units per milliliter (CFU/mL), unless differently specified. Note that colony counting was performed after cell redispersion in deionized water to ensure cell viability.

The evaporation of all droplets was carried out placing a droplet of 5–10  $\mu\text{L} \pm 4 \mu\text{L}$  on the epoxy substrates. For droplets containing bacteria, experiments were performed in triplicates drying 5 droplets over substrates independently. The images were collected with a CMOS camera PCO Sencicam at 1 frames per second (fps). The droplet completely evaporated in approximately  $2100 \pm 300$  s. Evaporation experiments were assessed at room temperature ( $21 \pm 3$  °C) in an atmosphere with a relative humidity of  $35 \pm 5\%$ .

The contact angle measurements of water and bacterial suspension droplets on epoxy surfaces were carried out by placing a water droplet with bacterial suspension of  $10^7$  CFU/mL on the epoxy substrates. The contact angle (CA) for H15 was  $100^\circ \pm 7^\circ$ , whereas the CA was  $92^\circ \pm 5^\circ$  for H22, H28, and H33. For longer pillars like H38 and H45, the CA was  $88^\circ \pm 3^\circ$ . CA hysteresis was carried out in a similar manner as CA measurements but by tilting the substrate  $45^\circ$ . Experiments were performed for the H15 substrate with and without bacterial containing droplets only, the CA hysteresis was  $50^\circ \pm 8^\circ$ . No significant differences in CA and CA hysteresis were observed between water droplets and the deposited bacterial containing droplets. CA values are shown in Table S1.

Transmission light microscopy images of the dried patterns were collected with a Zeiss 510 confocal microscope equipped with  $\times 10$ ,  $\times 20$ , and  $\times 40$  air objectives. AFM measurements from the Supporting Information were obtained using a Bruker Multimode 8 and a Keysights 5500 instrument. Prior to AFM morphological analysis, a droplet of bacteria suspension ( $10^7$  CFU/mL) was deposited onto an oxygen plasma-treated epoxy flat substrate and dried at room temperature. Estimated length ( $L$ )  $\times$  width ( $W_a$ ) in Table 1 are reported within a standard deviation of 10–25% obtained by measuring 15–20 cells per bacterial strains. These tests were carried out independently in triplicates. Top-view scanning electron microscopy (SEM) imaging was performed at 20 kV. Side-view SEM was recorded after fracturing the epoxy/glass with a diamond cutter at accelerating voltages of 3 kV. Prior to SEM inspection in a JSM-6610 JEOL system, all samples were coated with 20 nm of chromium to increase the electrical conductivity. SEM images are presented without fixation, which involves several solvent exchange steps<sup>39</sup> preserving the bacterial footprints after droplet evaporation.

## ASSOCIATED CONTENT

### Supporting Information

The Supporting Information is available free of charge on the ACS Publications website at DOI: 10.1021/acsabm.8b00176.

SEM images of some of the pillared arrays fabricated; AFM images of bacterial cells dried over flat epoxy

374 surfaces; close-ups of *E.coli* dried over the H15 pillared  
375 substrate; additional SEM images of bacteria on H15  
376 pillared structures; contact angle values for water and  
377 bacterial suspensions on different pillared structures  
378 (PDF)  
379 Video S1: droplet contour impalement (AVI)  
380 Video S2: pillar bending by *B. subtilis* at the latest stages  
381 of evaporation (AVI)

## 382 ■ AUTHOR INFORMATION

### 383 Corresponding Authors

384 \*E-mail: A.Susarrey-Arce@liverpool.ac.uk.

385 \*E-mail: Jose.HernandezSanchez@kaust.edu.sa.

386 \*E-mail: j.h.snoeijer@utwente.nl.

387 \*E-mail: r.raval@liverpool.ac.uk.

### 388 ORCID

389 Arturo Susarrey-Arce: 0000-0003-2572-223X

390 Detlef Lohse: 0000-0003-4138-2255

391 Han Gardeniers: 0000-0003-0581-2668

### 392 Author Contributions

393 <sup>○</sup>A.S.-A. and J.F.H.-S. contributed equally to this work

### 394 Notes

395 The authors declare no competing financial interest.

## 396 ■ ACKNOWLEDGMENTS

397 We would like to thank Dr. Joanna Wnetrzak and the  
398 Liverpool Centre for Cell Imaging (CCI) for help with  
399 experimental design and technical support. We also acknowl-  
400 edge the support of the Nanoinvestigation Centre at University  
401 of Liverpool (NICAL) for access to the SEM facility. Stefan  
402 Schlautmann (Mesoscale Chemical Systems, MESA+ Institute  
403 of Nanotechnology, University of Twente) is also acknowl-  
404 edged for sample fabrication. This work was partly funded by  
405 BBSRC (BB/R012415/1).

## 406 ■ REFERENCES

407 (1) Tawfik, S.; De Volder, M.; Copic, D.; Park, S. J.; Oliver, C. R.;  
408 Polsen, E. S.; Roberts, M. J.; Hart, A. J. Engineering of Micro-and  
409 Nanostructured Surfaces with Anisotropic Geometries and Properties.  
410 *Adv. Mater.* **2012**, *24*, 1628–1674.  
411 (2) Le, V.; Lee, J.; Chaterji, S.; Spencer, A.; Liu, Y.-L.; Kim, P.; Yeh,  
412 H.-C.; Kim, D.-H.; Baker, A. B. Syndecan-1 in Mechanosensing of  
413 Nanotopological Cues in Engineered Materials. *Biomaterials* **2018**,  
414 *155*, 13–24.  
415 (3) Chakrapani, N.; Wei, B.; Carrillo, A.; Ajayan, P. M.; Kane, R. S.  
416 Capillarity-Driven Assembly of Two-Dimensional Cellular Carbon  
417 Nanotube Foams. *Proc. Natl. Acad. Sci. U. S. A.* **2004**, *101*, 4009–  
418 4012.  
419 (4) Boesel, L. F.; Greiner, C.; Arzt, E.; Del Campo, A. Gecko-  
420 Inspired Surfaces: a Path to Strong and Reversible Dry Adhesives.  
421 *Adv. Mater.* **2010**, *22*, 2125–2137.  
422 (5) Prieto-López, L.; Williams, J. Using Microfluidics to Control Soft  
423 Adhesion. *J. Adhes. Sci. Technol.* **2016**, *30*, 1555–1573.  
424 (6) Prieto-López, L. O.; Williams, J. A. Switchable Adhesion Surfaces  
425 with Enhanced Performance Against Rough Counterfaces. *Biomimetics*  
426 **2016**, *1*, 2.  
427 (7) Kwak, M. K.; Jeong, H.-E.; Kim, T.-i.; Yoon, H.; Suh, K. Y. Bio-  
428 Inspired Slanted Polymer Nanohairs for Anisotropic Wetting and  
429 Directional Dry Adhesion. *Soft Matter* **2010**, *6*, 1849–1857.  
430 (8) Trichet, L.; Le Digabel, J.; Hawkins, R. J.; Vedula, S. R. K.;  
431 Gupta, M.; Ribault, C.; Hersen, P.; Voituriez, R.; Ladoux, B.  
432 Evidence of a Large-Scale Mechanosensing Mechanism for Cellular  
433 Adaptation to Substrate Stiffness. *Proc. Natl. Acad. Sci. U. S. A.* **2012**,  
434 *109*, 6933–6938.

(9) Liu, K.; Jiang, L. Bio-Inspired Design of Multiscale Structures for  
Function Integration. *Nano Today* **2011**, *6*, 155–175. 436  
(10) Asayesh, F.; Zarabadi, M. P.; Greener, J. A New Look at  
Bubbles During Biofilm Inoculation Reveals Pronounced Effects on  
Growth and Patterning. *Biomicrofluidics* **2017**, *11*, 064109. 437  
(11) Dean, B.; Bhushan, B. Shark-Skin surfaces for Fluid-Drag  
Reduction in Turbulent Flow: a Review. *Philos. Trans. R. Soc., A* **2010**,  
368, 4775–4806. 438  
(12) Guo, Z.; Liu, W. Biomimic from the Superhydrophobic Plant  
Leave in Nature: Binary Structure and Unitary Structure. *Plant Sci.* **2007**,  
172, 1103–1112. 439  
(13) Feng, L.; Zhang, Y.; Cao, Y.; Ye, X.; Jiang, L. The Effect of  
Surface Microstructures and Surface Compositions on the Wett-  
abilities of Flower Petals. *Soft Matter* **2011**, *7*, 2977–2980. 440  
(14) Fratzl, P.; Barth, F. G. Biomaterial Systems for Mechanosensing  
and Actuation. *Nature* **2009**, *462*, 442–448. 441  
(15) Bico, J.; Roman, B.; Moulin, L.; Boudaoud, A. Adhesion:  
Elastocapillary Coalescence in Wet Hair. *Nature* **2004**, *432*, 690–690. 442  
(16) Yeh, Y.-H.; Cho, K.-H.; Chen, L.-J. Effect of Softness of  
Polydimethylsiloxane on the Hydrophobicity of Pillar-Like Patterned  
Surfaces. *Soft Matter* **2012**, *8*, 1079–1086. 443  
(17) Nill, P.; Goehring, N.; Loeffler, R.; Peschel, A.; Kern, D. P.  
Studying Bacterial Adhesion Forces: Staphylococcus Aureus on  
Elastic Poly (Dimethyl) Siloxane Substrates. *Microelectron. Eng.* **2011**,  
88, 1825–1827. 444  
(18) Pokroy, B.; Kang, S. H.; Mahadevan, L.; Aizenberg, J. Self-  
Organization of a Mesoscale Bristle Into Ordered, Hierarchical  
Helical Assemblies. *Science* **2009**, *323*, 237–240. 445  
(19) Chandra, D.; Yang, S. Stability of High-Aspect-Ratio Micro-  
pillar Arrays Against Adhesive and Capillary Forces. *Acc. Chem. Res.* **2010**,  
43, 1080–1091. 446  
(20) Chandra, D.; Yang, S. Capillary-Force-Induced Clustering of  
Micropillar Arrays: is it Caused by Isolated Capillary Bridges or by the  
Lateral Capillary Meniscus Interaction Force? *Langmuir* **2009**, *25*,  
10430–10434. 447  
(21) Roman, B.; Bico, J. Elasto-Capillarity: Deforming an Elastic  
Structure with a Liquid Droplet. *J. Phys.: Condens. Matter* **2010**, *22*,  
493101. 448  
(22) Marchand, A.; Weijs, J. H.; Snoeijer, J. H.; Andreotti, B. Why is  
Surface Tension a Force Parallel to the Interface? *Am. J. Phys.* **2011**,  
79, 999–1008. 449  
(23) Weijs, J. H.; Andreotti, B.; Snoeijer, J. H. Elasto-Capillarity at  
the Nanoscale: on the Coupling between Elasticity and Surface  
Energy in Soft Solids. *Soft Matter* **2013**, *9*, 8494–8503. 450  
(24) Yang, M. T.; Fu, J.; Wang, Y.-K.; Desai, R. A.; Chen, C. S.  
Assaying Stem Cell Mechanobiology on Microfabricated Elastomeric  
Substrates with Geometrically Modulated Rigidity. *Nat. Protoc.* **2011**,  
6, 187–213. 451  
(25) Wei, Z.; Schneider, T.; Kim, J.; Kim, H.-Y.; Aizenberg, J.;  
Mahadevan, L. Elasto-capillary Coalescence of Plates and Pillars. *Proc.*  
*R. Soc. London, Ser. A* **2015**, *471*, 20140593. 452  
(26) Ledesma-Aguilar, R.; Laghezza, G.; Yeomans, J. M.; Vella, D.  
Using Evaporation to Control Capillary Instabilities in Micro-  
Systems. *Soft Matter* **2017**, *13*, 8947–8956. 453  
(27) Jahed, Z.; Shahsavan, H.; Verma, M. S.; Rogowski, J. L.; Seo, B.  
B.; Zhao, B.; Tsui, T. Y.; Gu, F. X.; Mofrad, M. R. K. Bacterial  
Networks on Hydrophobic Micropillars. *ACS Nano* **2017**, *11*, 675–  
683. 454  
(28) Chew, S. C.; Kundukad, B.; Teh, W. K.; Doyle, P.; Yang, L.;  
Rice, S. A.; Kjelleberg, S. Mechanical Signatures of Microbial Biofilms  
in Micropillar-Embedded Growth Chambers. *Soft Matter* **2016**, *12*,  
5224–5232. 455  
(29) Biais, N.; Ladoux, B.; Higashi, D.; So, M.; Sheetz, M.  
Cooperative Retraction of Bundled Type IV Pili Enables Nanonewton  
Force Generation. *PLoS Biol.* **2008**, *6*, 1–7. 456  
(30) Ng, D.; Harn, T.; Altindal, T.; Kolappan, S.; Marles, J. M.; Lala,  
R.; Spielman, I.; Gao, Y.; Hauke, C. A.; Kovacicova, G.; Verjee, Z.;  
Taylor, R. K.; Biais, N.; Craig, L. The *Vibrio cholerae* Minor Pili 501

- 503 TcpB Initiates Assembly and Retraction of the Toxin-Coregulated  
504 Pilus. *PLoS Pathog.* **2016**, *12*, 1–31.
- 505 (31) Susarrey-Arce, A.; Marin, A.; Massey, A.; Oknianska, A.; Díaz-  
506 Fernandez, Y.; Hernández-Sánchez, J. F.; Griffiths, E.; Gardeniers, J.  
507 G. E.; Snoeijer, J. H.; Lohse, D.; Raval, R. Pattern Formation by  
508 Staphylococcus Epidermidis via Droplet Evaporation on Microoillars  
509 Arrays at a Surface. *Langmuir* **2016**, *32*, 7159–7169.
- 510 (32) Hochbaum, A. I.; Aizenberg, J. Bacteria Pattern Spontaneously  
511 on Periodic Nanostructure Arrays. *Nano Lett.* **2010**, *10*, 3717–3721.
- 512 (33) Li, X.; Cheung, G. S.; Watson, G. S.; Watson, J. A.; Lin, S.;  
513 Schwarzkopf, L.; Green, D. W. The Nanotipped Hairs of Gecko Skin  
514 and Biotemplated Replicas Impair and/or Kill Pathogenic Bacteria  
515 with High Efficiency. *Nanoscale* **2016**, *8*, 18860–18869.
- 516 (34) Kim, P.; Epstein, A. K.; Khan, M.; Zarzar, L. D.; Lipomi, D. J.;  
517 Whitesides, G. M.; Aizenberg, J. Structural Transformation by  
518 Electrodeposition on Patterned Substrates (STEPS): A New Versatile  
519 Nanofabrication Method. *Nano Lett.* **2012**, *12*, 527–533.
- 520 (35) Pokroy, B.; Epstein, A. K.; Persson-Gulda, M. C. M.; Aizenberg,  
521 J. Fabrication of Bioinspired Actuated Nanostructures with Arbitrary  
522 Geometry and Stiffness. *Adv. Mater.* **2009**, *21*, 463–469.
- 523 (36) Hadjittofis, A.; Lister, J. R.; Singh, K.; Vella, D. Evaporation  
524 Effects in Elastocapillary Aggregation. *J. Fluid Mech.* **2016**, *792*, 168–  
525 185.
- 526 (37) Haiko, J.; Westerlund-Wikström, B. The Role of the Bacterial  
527 Flagellum in Adhesion and Virulence. *Biology* **2013**, *2*, 1242–1267.
- 528 (38) Hizal, F.; Choi, C.-H.; Busscher, H. J.; van der Mei, H. C.  
529 Staphylococcal Adhesion, Detachment and Transmission on Nano-  
530 pillared Si Surfaces. *ACS Appl. Mater. Interfaces* **2016**, *8*, 30430–  
531 30439.
- 532 (39) Susarrey-Arce, A.; Sorzabal-Bellido, I.; Oknianska, A.; McBride,  
533 F.; Beckett, A. J.; Gardeniers, J. G. E.; Raval, R.; Tiggelaar, R. M.; Diaz  
534 Fernandez, Y. A. Bacterial Viability on Chemically Modified Silicon  
535 Nanowire Arrays. *J. Mater. Chem. B* **2016**, *4*, 3104–3112.